An Experimental/Computational Approach to Identify Moduli and Residual Stress in MEMS Radio-Frequency Switches

by H.D. Espinosa, Y. Zhu, M. Fischer, and J. Hutchinson

ABSTRACT—In this paper, we identify the Young's modulus and residual stress state of a free-standing thin aluminum membrane, used in MEMS radio-frequency (rf) switches. We have developed a new methodology that combines a membrane deflection experiment (MDE) and three-dimensional numerical simulations. Wafer-level MDE tests were conducted with a commercially available nanoindenter. The accuracy and usefulness of the MDE is confirmed by the repeatability and uniformity of measured load–deflection curves on a number of switches with both wedge and Berkovich tips. It was found that the load–deflection behavior is a function of membrane elastic properties, initial residual stress state and corresponding membrane shape. Furthermore, it was assessed that initial membrane shape has a strong effect on load–deflection curves; hence, its accurate characterization is critical. Through an iterative process and comparison between MDE data and numerical simulations, the Young's modulus and residual stress state, consistent with measured membrane shape, were identified. One important finding from this investigation is that variations in membrane elastic properties and residual stress state affect the load–deflection curve in different regimes. Changes in residual stress state significantly affect the load–deflection slope at small values of deflection. By contrast, variations in Young's modulus result in changes in load–deflection slope at large deflections. These features are helpful to decouple both effects in the identification process.

KEY WORDS—MEMS, rf switch, moduli, residual stress, nanoindentation

Introduction

Microelectromechanical systems (MEMS) are one of the most significant technological advances of this decade. This technology employs systems with dimensions of only a few hundred micrometers. Applications ranging from drug delivery systems to telecommunications are currently under research and development. Their reduced size and mass give them unique technological advantages. For instance, radio-frequency (rf) switches used in wireless applications exhibit microsecond time responses, low insertion losses and low power consumption. However, size reduction also results in mechanical characterization challenges.

The impact of the technology is such that during the first few months of 2001 three feature articles appeared in the IEEE Spectrum[1,2] and Mechanical Engineering magazines.[3] In all of these articles, the problem of MEMS reliability, due to lack of fundamental understanding of failure mechanisms, is highlighted as a major limitation for the commercialization of MEMS devices. Key problems to be solved are packaging and mechanical modeling of MEMS materials at the micrometer scale. For instance, in the case of rf switches, the effect of the environment can result in stiction of the membranes due to humidity or other sources. From a reliability point of view, it is necessary to consider the plasticity limit and its dependence with temperature of the materials involved. Temperatures as low as –50°C can be reached in satellite and airplane wireless applications while temperatures of a few hundred degrees can be present during packaging of the device. Another possible failure mechanism is fatigue due to a large accumulation of actuation cycles. Most of these devices are typically actuated at very large number of cycles pushing the design envelope and our current knowledge of material behavior beyond known parameters.

In this paper, we address the identification of the Young's modulus and residual stress state of free-standing membranes used in the design of MEMS rf switches. We begin with a description of the MEMS rf switch investigated in this study. Then, limitations of currently available experimental techniques are discussed and a new test is presented. A subsequent section refers to three-dimensional numerical simulations carried out to identify the device residual stress state and the material Young's modulus. The initial shape of the free-standing membranes is taken into account. Finally, we give conclusions arising from the combined experimental–computational methodology and its applicability to the study of MEMS reliability.

The MEMS rf Switch

Goldsmith et al.[4–7] have reported on MEMS rf switches employing free-standing metal membranes, with capacitive coupling. The side-view architecture of one such MEMS switch is shown in Fig. 1(a). The switches are manufactured on a GaAs substrate, over which a "bow-tie" metal membrane is deposited by evaporation. The material used in the membrane is an aluminum alloy. This membrane is the only moving part of the device. Its shape, size and mechanical

H.D. Espinosa (espinosa@northwestern.edu) (SEM Member) is a Professor, Y. Zhu is a Graduate Student, and M. Fischer is a Graduate Student, Northwestern University, Evanston, IL 60208-3111. J. Hutchinson is a Professor, Harvard University, Cambridge, MA 02138.

Original manuscript submitted: December 19, 2002.
Final manuscript received: December 19, 2002.

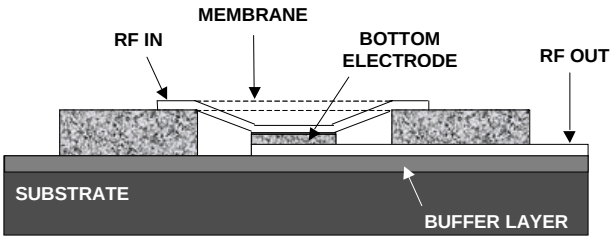

(a)

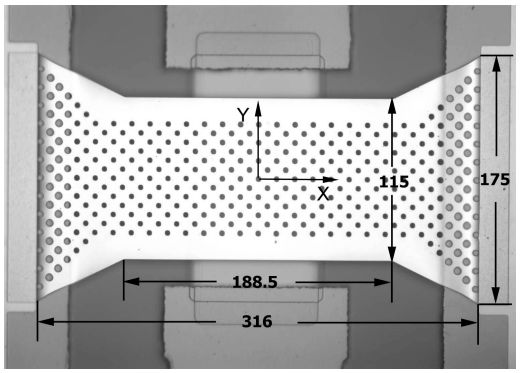

(b)

Fig. 1—(a) Cross-section of MEMS rf switch. (b) Optical micrograph of the "bow-tie" membrane mounted on posts. The membrane is made of aluminum alloy and contains a pattern of holes for membrane release during plasma etching. All dimensions are in micrometers.

properties determine the behavior of the MEMS switch. Two of its edges are attached to thin posts that maintain it suspended over an insulated electrode. Microfabrication details and employed materials have been reported by Goldsmith et al.[4,6] Switching is achieved by applying a pulling-in voltage between the membrane and the bottom electrode.

Figure 1(b) shows the top view of a switch together with its dimensions. The membrane thickness is 300 nm with a variability of ± 10 nm from membrane to membrane. The gray circular dots over the membrane are small holes, 2 μm in diameter, which are necessary for plasma etching of the polymer–sacrificial layer. These holes also play a role in the dynamic behavior of the switch, by providing viscous damping, if actuated in an inert gas or air.

Methodology

A review of the literature was carried out to identify an experiment suitable for the identification of the membrane Young's modulus and residual stress state. Among the most established experimental techniques, we can cite the bulge test,[8–10] the microtensile test developed by Sharpe et al.[11–14] and nanoindentation,[15–19] especially the deflection of circular membranes.[20] The bulge, microtensile tests and circular membrane deflection techniques require the microfabrication of special specimens. In view of the fact that the metal membrane grain structure and residual stress state are highly dependent on the substrate material and fabrication steps, the usage of specially designed samples was not deemed appropriate. Likewise, we found indentation tests performed on areas of the membrane on top of the posts very unreliable. Strong depth dependence was measured and the modulus and hardness never reached a constant value, see Fischer[21] and Espinosa et al.[22] The unsuitability of these experimental methodologies for the device under investigation prompted us to develop a new combined experimental–computational methodology.

A wafer-level experimental technique was employed together with three-dimensional numerical simulations of the experiments.[23] The overall experimental/computational approach consisted of:

- membrane characterization, to measure dimension and topography using optical full field profilometry;
- membrane deflection experiments (MDEs), to interrogate the structural response of the device;
- three-dimensional finite element analysis (FEA), to correlate the experimentally measured load–deflection curves.

Making use of a nanoindenter (MTS Co.), MDEs were performed to investigate the membrane structural response. The technique should not be confused with nanoindentation or with microbending of cantilevers or fixed–fixed beams.[17,24] Since the sample is attached to the posts along two of its edges, and a gap of about 4 μm exists under the membrane, a load–deflection measurement was used to interrogate the membrane elastic response. The experiment consisted of applying either a point or a line load in the middle of the span of the fixed–fixed membrane. A specially designed 125 μm long diamond wedge tip and a Berkovitch tip were used to apply the loads. The idea of using two tip geometries was to examine the sensitivity of the approach to load geometry as well as to obtain redundant experimental information. By deflecting the membrane down, information on both elastic behavior and residual stress state was obtained. Obviously the structural response was coupled, so analysis was needed to decouple the effects.

The experiment was quite challenging because the stiffness of the specimen, about 10 N m^{-1}, is only 10% that of the nanoindenter column stiffness in air, which is approximately 100 N m^{-1}. Furthermore, thermal drift is part of the measured load signature. However, the nanoindenter is capable of acquiring load and displacement with high resolution and to perform several pre-programmed steps on the same or different membranes. Hence, we were able to develop a procedure for removing spring and thermal drift effects in the load signature, which proved to be quite robust and accurate.[21,25] Loads with a resolution of a fraction of a μN and displacements with a resolution of less than a nanometer were so measured.

The protocol normally used in nanoindentation tests was employed in these MDEs. Two positioning indentations, over the posts, were first made to measure device tilt, membrane height in the middle of the span, and to accurately determine the center load location. This positioning was carried out with

an accuracy of less than 1 μm, which is less than 0.32% of the membrane span. The device tilt was adjusted until the indentation marks left by the wedge tip, over the posts, had uniform depth. A thermal drift check, below a desired value, was performed before the start of the loading phase.

The set of parameters employed in the experiments was: surface search distance = 6000 μm, radius to initial impact = 50 μm, angle to initial impact = 80°, maximum drift rate prior to tests = 1 nm s^{-1}, and tip displacement rate = 10 nm s^{-1}. The surface search distance is the distance above the sample at which the approach stage begins. For these membranes, a long approach (6 μm) was used due to surface curvature. A large number of data points, during the approach stage, were recorded in order to be able to characterize the change in stiffness when the tip contacted the membrane. The tip approach rate was 60 nm s^{-1} until it reached the bottom electrode, where the tip displacement rate was changed to 10 nm s^{-1} to avoid large load increases that could damage the device.

The FEA analyses were carried out in two steps. The first step assumed values of Young's modulus, uniform uniaxial stress and a first approximation to the membrane initial shape. The solution of this step resulted in an equilibrium non-uniform stress state and a compatible membrane geometry, which was compared to the measured one. This first step was performed iteratively until the computed and measured membrane geometries agreed to within a set error. The error norm used in the calculations is reported in the following section. The second step simulated the motion of the nanoindenter tip and computed the interaction force between tip and membrane. A load–deflection response was so computed.

Results and Discussion

The rf MEMS Membrane Metrology

Prior to the MDE tests, a careful characterization of the membrane dimensions and out-of-plane initial shape was carried out. The in-plane dimensions of the investigated rf switch are given in Fig. 1(b). The membrane presents a bow-tie shape necessary for optimal switch performance. The total membrane span is 316 μm and its width varies from 175 to 115 μm. The hole pattern and diameter of 2 μm were also measured to include them into the solid model employed in the numerical simulations.

The membrane surface was scanned using the MicroXAM 3D surface profiler system. The measured membrane topography exhibited waviness along the span in both directions. The measured membrane shape can be mathematically described by the following function

$$Z(x, y) = A \cos\left(\frac{5\pi x}{L}\right) \cos\left(\frac{0.8\pi x}{L}\right) \cos\left(\frac{\pi y}{W}\right), \quad (1)$$

where A is the amplitude, L is the length of the membrane and W is the width. The average amplitude was found to be 0.2 μm. Measurements on several membranes show similar topography with minor variations in the magnitude of the curvatures. As will be shown later, this initial membrane shape plays an important role in the proper identification of membrane mechanical properties.

A focused ion beam (FIB) was employed to characterize the film material grain size and membrane thickness. An image taken from a sectioned membrane is shown in Fig. 2. The micrograph shows grain morphology and size immediately after sectioning and etching of a native oxide layer. A 20 nm thick native oxide layer can be observed in Fig. 2. A single grain through the thickness with a columnar morphology is also clearly observed. The average grain size is about 250 nm. Note that the sample is tilted 45° to better image the grains.

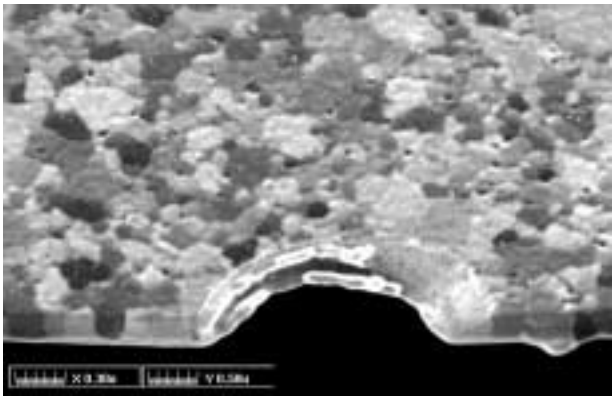

Fig. 2—Image showing the grains of the aluminum alloy membrane after removing a top thin oxide layer. The bottom oxide layer is observed as a thin lighter border along the edge. The sectioning was performed using a FIB. The average grain size is about 250 nm and the membrane thickness is 300 nm with only one grain through the thickness.

Membrane Deflection Experiments

Figure 3(a) shows experimental results, obtained by testing one switch through repeated loading. The four tests were conducted employing a wedge tip. Contact with the membrane is taken as the zero displacement. As previously explained, the membrane response to stretching was obtained, as it was pulled down by a displacement equal to the gap. When the bottom electrode was reached, we observed a steep increase in load, corresponding to a large stiffness increase. The membrane was not damaged as a result of the test, and no mark was found after it. The repeatability of the test is clearly demonstrated in view of the small variations in the recorded load–deflection curves.

The same deflection experiment was conducted on four different switches to examine wafer uniformity. The measured load–deflection curves are shown in Fig. 3(b). A very small spread in the experimental curves is observed, indicative that the microfabrication process is quite uniform over the wafer. Small variations in maximum deflection prior to contact with the bottom electrode are also observed, which is consistent with the variation in membrane initial shape.

Similar experimental results were obtained when a concentrated force, using a Berkovich tip, was applied at the center of the membrane. The load–displacement signatures, Figs. 4(a) and (b), again confirm the test repeatability and switch uniformity across the wafer. In all cases very small unloading events are recorded along the deflection process. It was determined, by examining the nanoindenter column motion in air, that such perturbations may be the result of the nanoindenter column behavior rather than true device behavior. However, another possibility is slipping of the tip as a result of membrane local deformation associated to its initial

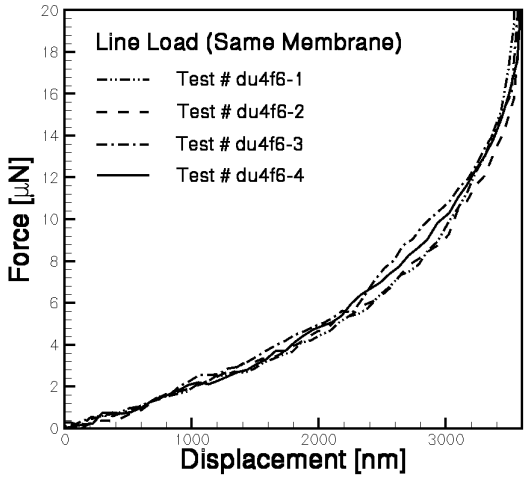

(a)

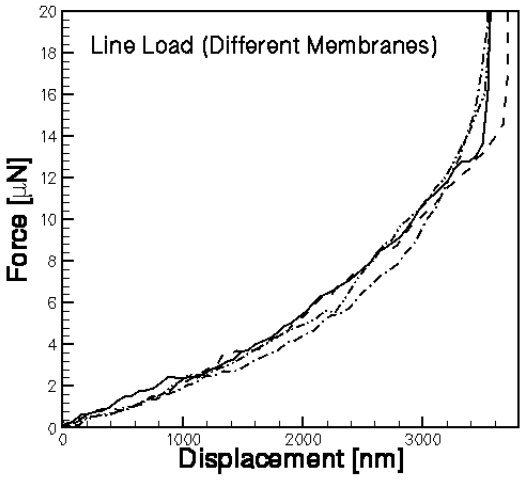

(b)

Fig. 3—(a) MDE curves obtained from a single membrane repeatedly tested using a wedge tip. Repeatability is observed. (b) MDE curves on four different membranes using a wedge tip. Small variability among rf switches is observed.

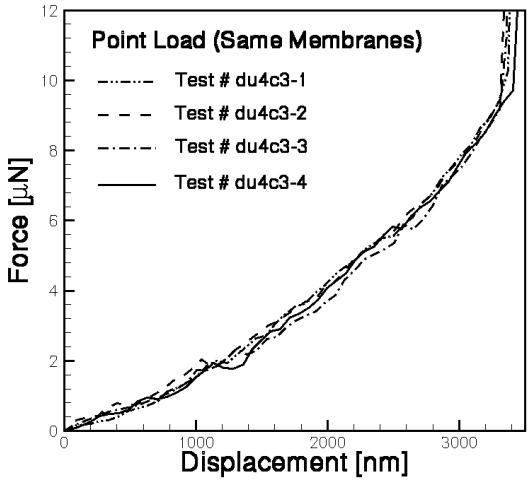

(a)

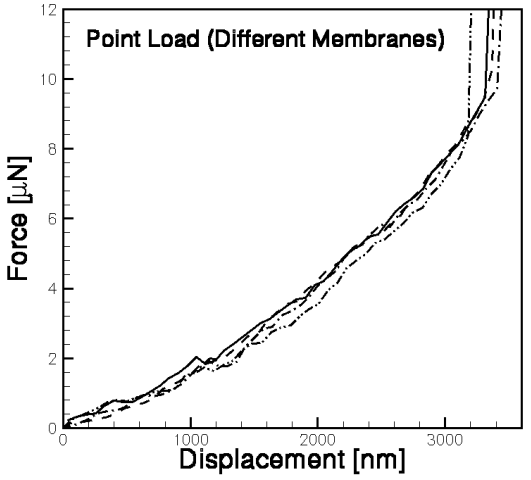

(b)

Fig. 4—(a) MDE curves obtained from a single membrane repeatedly loaded using a Berkovich tip. Repeatability is observed. (b) MDE curves on four different membranes using a Berkovich tip. Small variability among the rf switches is observed.

waviness. It should be noted that the instrument is used at the limit of its resolution.

Numerical Simulations

The membrane deflection experiment was simulated using the finite element software ABAQUS Standard, version 5.8. The simulation consisted of a quasi-static three-dimensional contact problem with the tip modeled as a rigid body and the fixed–fixed membrane as a shell attached along its edges, i.e., $Z(\pm L/2, y) = 0$. The edges of the membrane along the posts were fixed to simulate the bonding between membrane and posts. The membrane was discretized using eight-noded shell elements with variable dimensions in the x–y plane and a constant thickness of 300 nm in the z-direction. The element type used to model the membrane was the S8R5. The diamond wedge tip was modeled as a rigid body with a tip radius of 40 nm and 80° incline angles. The element type R3D4 was employed in discretizing the tip. The rigid element nodes were master nodes in the contact pair while the shell elements defined the slave surface. The mesh is shown in Fig. 5 for both loading types. The figure is a zoom of the tip and membrane. A very fine mesh is used to define the contact area under the tip.

Nonlinear kinematics was included in the simulations to examine the changes in membrane stiffness with deflection. Material plasticity was not accounted for since, at maximum deflection, the stress state everywhere in the membrane was below the material yielding stress. The numerical analysis was performed in two steps. The first step consisted of solving the system of governing equations for an initial uniform uniaxial stress and a first approximation of the initial membrane shape. Equilibrium resulted in a new membrane

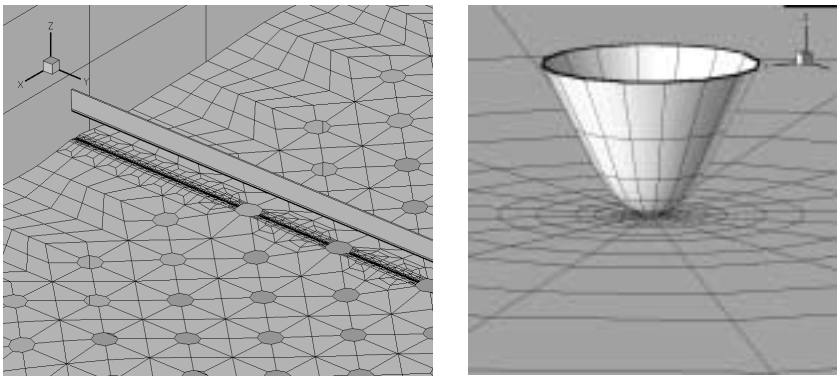

Fig. 5—Plot of line (wedge tip) and point load (Berkovitch tip) finite element meshes in the contact region. A refined mesh was used in the contact area to capture local bending and tip geometry.

shape and a non-uniform biaxial stress distribution. The second step consisted of applying a prescribed displacement to the tip. The prescribed displacement rate was the same as that used in the experiment, although this was not necessary considering that the simulation was quasi-static. The contact load was an outcome of the calculation dependent on the membrane behavior.

In order to analyze the sensitivity of the membrane structural response to variations in Young's modulus, the model was examined with four values of E at a fixed initial uniaxial stress of 10 MPa. A flat membrane was used in these simulations. The bulk modulus of aluminum, 73.2 GPa (10.6×10^6 psi), and three smaller values, 50, 45, and 40 GPa, were examined. In all calculations, a Poisson's ratio of 0.34 was used. The simulated load–displacement behaviors are shown in Fig. 6(a). Considering that a variation of 33.2 GPa in E is examined, the differences in load–deflection curves are modest, and almost negligible at small values of deflection. By contrast, the slope of the load–deflection curve varies significantly, for the various values of E, when the deflection reaches 3 μm.

To examine the effect of initial stress, σ_0, on the load–deflection curve, four simulations were performed with initial stress of 0, 5, 10, and 15 MPa. A fixed Young's modulus of E = 45 GPa and a flat membrane geometry were employed. The simulated load–displacement curves are shown in Fig. 6(b). It is interesting to note that the initial slope of the load–deflection curve is highly sensitive to the state of initial stress. In fact, higher values of initial stress translate in a tension stiffness that becomes evident even at small deflections. As mentioned in the previous paragraph, variations in Young's modulus have little effect in the stiffness of the membrane, when the deflections are small. These sensitivity features are very important to properly identify membrane moduli and initial residual stress, as it is the objective of this investigation.

The previously discussed analyses were all performed using a flat membrane. This is enough for the purpose of understanding the effects of E and σ_0 through the identification process. However, due to thermal and film deposition effects, the membranes in each switch have an initial wavy geometry. For the purpose of investigating this effect, several membrane topographies were analyzed, flat and wavy with two different

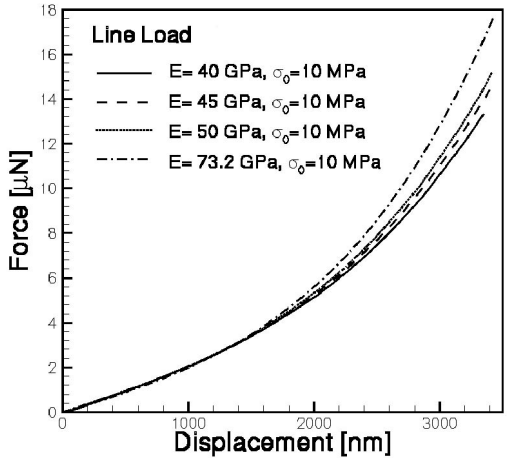

(a)

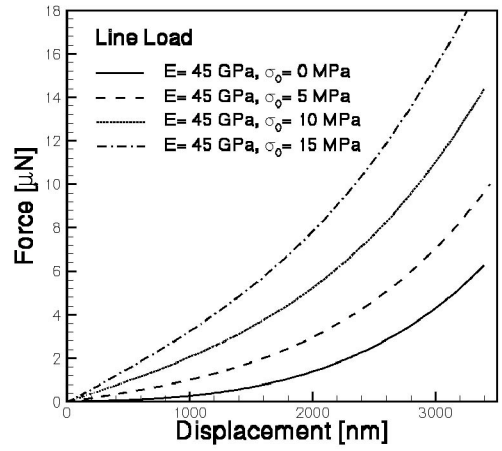

(b)

Fig. 6—(a) Effect of Young's modulus on load-deflection response. (b) Effect of residual stress on load-deflection response. The membrane shape is flat in all these simulations.

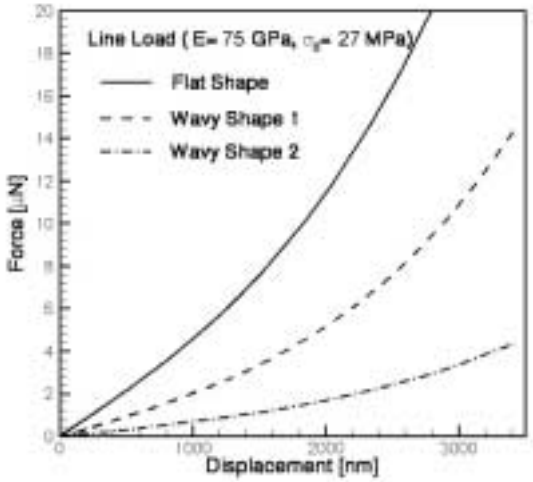

Fig. 7—Effect of initial membrane shape on load-deflection behavior. The shape function for the wavy shape is shown in eq (1). For wavy shape 1, the amplitude is 0.2 μm; for wavy shape 2, the amplitude is 0.4 μm.

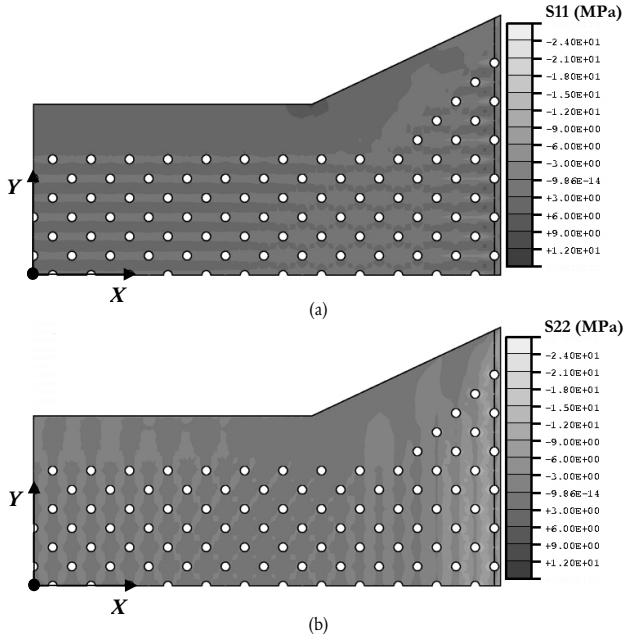

Fig. 8—(a) Contour plot of Cauchy stress S11 in the local 11 direction for E = 75 GPa and uniform initial stress σ_0 = 27 MPa. (b) Contour plot of Cauchy stress S22 in the local 22 direction. Due to the symmetry of membrane geometry and loading, only a quarter of the membrane is shown. Note that the local 11 direction is the projection of the global X-axis onto the membrane surface, and the local 22 direction is at right angles to the local 11 direction. In most of the membrane except for the edge area, S11 is between 0 and 6 MPa, and S22 is between –3 and 3 MPa.

amplitudes (0.2 and 0.4 μm). The load–deflection curves for these cases are shown in Fig. 7 as calculated for an initial stress of 27 MPa. Significant changes in load–deflection behavior are observed with the flat membrane geometry being the stiffer, as would be expected. The effect of the amplitude of the waviness is illustrated when wavy shapes 1 and 2 are compared. These simulations demonstrate that the model must accurately capture the initial shape of the membrane.

The above sensitivity study shows that the identification process involves three variables: initial membrane shape, initial stress, and Young's modulus (S, σ_0, E). While the effects of σ_0 and E can be decoupled, by examining the stiffness of the membrane at zero and maximum deflection, the initial membrane shape affects the membrane stiffness in both deformation regimes and, therefore, the identification of both parameters. As a result we have performed the identification of (S, σ_0, E) through an iterative process.

We next report on the convergent solution for both steps of the analysis. The first step of the FEA analysis was carried out by assuming a Young's modulus (E), an initial assumed shape (S) and a uniaxial uniform stress (σ_0). Clearly this initial state did not satisfy equilibrium. By solving the governing equations for the discrete system, a solution with a non-uniform biaxial stress distribution and a new membrane shape was obtained. As a criterion of solution convergence, we employed an error norm given by

$$||e|| = [\sum_{i=1}^{n} (Z_{cal} - Z_{meas})^2]^{1/2} / Z_{\max}. \qquad (2)$$

Here, Z_{cal} is the numerically calculated Z coordinate of the membrane, Z_{meas} is the measured one given by eq (1), Z_{max} is the maximum measured Z coordinate and n is the number of mesh nodes.

Cauchy stress contours of S_{xx} and S_{yy} resulting from this analysis are shown in Figs. 8(a) and (b), for the case of an assumed uniform initial uniaxial stress of σ_0 = 27 MPa. For this calculation, an error $||e|| < 3\%$ was used. A large variation in calculated residual stress is observed as a function of position. In the relatively flat part of the membrane, the average residual stress in the X-direction is between 0 and 6 MPa. By contrast, close to the fixed ends, compressive stresses as high as 24 MPa are observed. The average residual stress in the Y-direction is between –3 and 3 MPa in the relatively flat part. These findings are in agreement with the non-uniform stress distribution reported by Chen et al.[26] for the same MEMS device.

The membrane shape and state of residual stress computed in the first step was used as initial condition for the second step of the FEA simulation. This second step consisted of applying a prescribed displacement to the nanoindenter tip while computing the contact force. The load–deflection curves resulting from this second step, for both line and concentrated loads, are shown in Fig. 9(a). The good correlation between simulations and experiments proves that the solution set, E = 75 GPa, computed initial shape and associated non-uniform biaxial stress state, provides an accurate mechanical description of the MEMS device. An important feature to note is that the same set of parameters precisely captures load–deflection signatures obtained with two different loading geometries. This provides confidence in the accuracy of the experimental measurements and identified parameters.

Fig. 9(b) shows the comparison between two simulations and the four experiments reported in Fig. 3. The simulations are for line load, with the upper curve for E = 80 GPa and the lower curve for E = 70 GPa. It is seen that the experimental

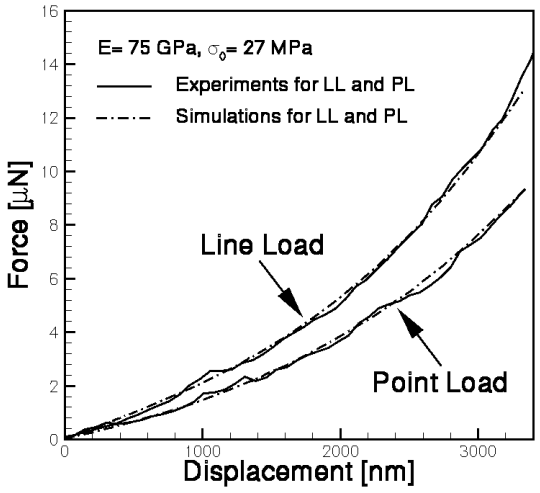

(a)

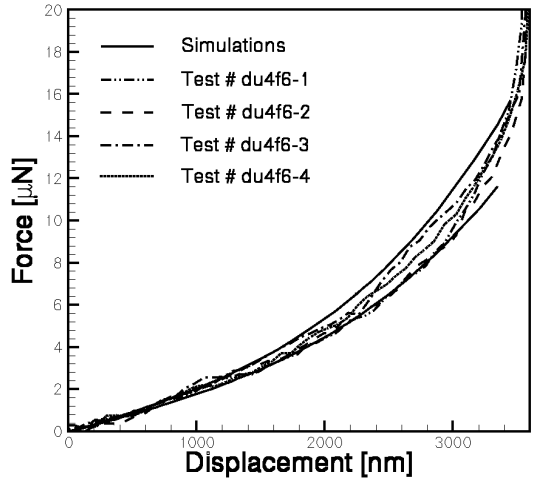

(b)

Fig. 9—(a) Comparison of numerical simulations with experiments for both line load and point load for E = 75 GPa and uniform initial stress σ_0 = 27 MPa. (b) Comparison of simulations with four experimental results. The upper solid line was obtained with E = 80 GPa and the lower solid line was obtained with E = 70 GPa. Both calculations were performed based on the same membrane shape and residual stress state.

curves lie between two simulations, which implies that E = 75 ± 5 GPa.

Conclusions

We have developed a procedure for the identification of the Young's modulus and residual stress state in thin aluminum membranes, employed in the design of MEMS rf switches. The strong dependence of these quantities on membrane shape, attachment to the substrate and microfabrication steps, severely restricted the selection of a suitable testing methodology. Microfabrication of specimens for bulge or microtension tests was ruled out for these reasons.

It was determined that the load–deflection response of these membranes is very sensitive to residual stress at small deflections. By contrast, the sensitivity to variations in the Young's modulus becomes important at large deflections. These findings have the implication that the effects of Young's modulus and residual stress state can be decoupled. Furthermore, it was shown that proper identification of Young's modulus and residual stress state requires that the initial shape of the membrane be taken into account. In our methodology, this was accomplished by performing membrane metrology and a two-step FEA analysis.

The MDE test proved to be very reliable even when a membrane stiffness of one order of magnitude smaller than the nanoindenter column stiffness was measured. To the best of our knowledge, the results reported here are the first of their kind. Performing several experiments on the same MEMS device repeatability of the test was assessed. In all loading cases, the scatter of the data was small. By performing the experiment on several switches, in the same wafer, the uniformity of the manufacturing process was identified. This feature and the fact that the test is performed at the wafer level, without the need of specially designed specimens and with a commercially available nanoindenter, are expected to be very valuable in quality control of MEMS devices in large-scale manufacturing processes.

A major remaining challenge in the design of MEMS devices is the capability to assess their reliability. For instance, MEMS rf switches are expected to be actuated by a large number of cycles in wireless or other applications. Problems associated to stiction, relaxation of residual stresses that control the time response of the device, through a spring back effect, or even material fatigue can be envisioned. The methodology presented here can be employed to address some of these problems. For instance, by electrostatically actuating the large number of cycles of the switches and by performing MDE experiments at periodic intervals, a complete evolution of residual stress state and mechanical properties can be investigated. Complementary TEM, FIB and scanning electron microscopy (SEM) studies performed on the tested devices could provide valuable insight into failure mechanisms at the microscale and, therefore, increase our ability to design microdevices.

Acknowledgments

The authors acknowledge the support of Raytheon Systems Co., through a grant to Northwestern University. HDE also acknowledges the support from NSF through a Young Investigator Award, NSF-Career Award No CMS-9624364, and FAA Award No DTFA03-01-C-00031. This work would have not been possible without the input and rf switches provided by T. Baughn, S. Chen, and C. Goldsmith of Raytheon Systems Co., Dallas, TX 75243. Special thanks are due to Warren Oliver and Erik Herbert, MTS Systems Nano Instruments Innovation Center, for providing valuable insight on the experimental process using the Nanoindenter XP.

References

1. Geppert, L., "RF Bridges to the Network," IEEE Spectrum Magazine, 69–71, (January 2001).

2. Cass, S., "Large Jobs for Little Devices," IEEE Spectrum Magazine, 72–73, (January 2001).

3. Chalmers, P., "Relay Races," Mechanical Engineering Magazine, 54–62 (January 2001).

4. Goldsmith, C., Lin, T., Powers, B., Wen, R., and Norvell, B., "Micromechanical Membrane Switches for Microwave Applications," IEEE Microwave Theory Tech. Symp., **1**, *91–94 (1995).*

5. Goldsmith, C., Yao, Z., Eshelman, S., and Denniston, D., "Performance of Low-loss RF MEMS Capacitive Switches," IEEE Microwave Guided Wave Lett., **8** *(8), 269–271 (1998).*

6. Goldsmith, C., Malczewski, A., Yao, Z., Chen, S., Ehmke, J., and Hinzel, D., "RF MEMS Variable Capacitors for Tunable Filters," Int. J. RF Microwave Computer-Aided Eng., **9** *(4), 362–374 (1999).*

7. Goldsmith, C., Randall, J., Eshelman, S., Lin, T., Denniston, D., Chen, S., and Norvell, B., "Characteristics of Micromachined Switches at Microwave Frequencies," IEEE Microwave Theory Tech. Symp., **2**, *1141–1144 (1996).*

8. Small, M. and Nix, W., "Analysis of the Accuracy of the Bulge Test in Determining the Mechanical Properties of Thin Films," J. Mater. Res., **7** *(6) (1992).*

9. Vlassak, J. and Nix, W., "A New Bulge Test Technique for the Determination of Young's Modulus and Poisson's Ratio of Thin Films," J. Mater. Res., **7** *(12) (1992).*

10. Small, M., Daniels, B., Clemens, B., and Nix, W., "The Elastic Biaxial Modulus of Ag–Pd Multilayered Thin Films Using the Bulge Test," J. Mater. Res., **9** *(1) (1994).*

11. Yuan, B. and Sharpe Jr., W., "Mechanical Testing of Polysilicon Thin Films With the ISDG," EXPERIMENTAL TECHNIQUES, **21** *(2), 32–35 (1997).*

12. Sharpe Jr., W., "A New Technique for Measuring Poisson's Ratio of MEMS Materials," Proc. Mater. Res. Soc. Symp., **444**, *185–190, Boston, MA (1996).*

13. Sharpe Jr., W., "ASME NADAI Lecture—Elastoplastic Stress and Strain Concentrations," J. Eng. Mater. Technol., **117**, *1–7 (1995).*

14. Zeng, H. and Sharpe Jr., W., "A System for Measuring Biaxial Creep Strains Over Short Gage Lengths," EXPERIMENTAL MECHANICS, **53**, *84–97 (1996).*

15. Shell de Guzman, M., Neubauer, G., Flinn, P., and Nix, W., "The Role of Indentation on the Measured Hardness of Materials," Proc. Mater. Res. Soc. Symp., **308**, *613–618 (1993).*

16. Nix, W., "Elastic and Plastic Properties of Thin Films on Substrates: Nanoindentation Techniques," Mater. Sci. Eng. A, **234–236**, *37–44 (1997).*

17. Baker, S. and Nix, W., "Mechanical Properties of Compositionally Modulated Au–Ni Thin Films: Nanoindentation and Microcantilever Experiments," J. Mater. Res., **9** *(12), 3131–3144 (1994).*

18. Tsui, T., Oliver, W., and Pharr, G., "Influences of Stress on the Measurement of Mechanical Properties Using Nanoindentation: Part I. Experimental Studies in an Aluminum Alloy," J. Mater. Res., **11** *(3), 752–759 (1996).*

19. Tsui, T., Oliver, W., and Pharr, G., "Influences of Stress on the Measurement of Mechanical Properties Using Nanoindentation: Part II. Finite Element Simulations," J. Mater. Res., **11** *(3), 760–768 (1996).*

20. Hong, S., Weihs, T.P., Bravman, J.C., and Nix, W.D., "Measuring Stiffness and Residual Stresses of Silicon Nitride Thin Film," J. Electron. Mater., **19**, *903–909 (1990).*

21. Fischer, M., "MEMS Material Testing," Masters of Science, Purdue University (1999).

22. Espinosa, H.D., Fischer, M., Herbert, E., and Oliver, W., "Identification of Residual Stress State in an RF-MEMS Device," white paper, MTS Systems Corporation (2001).

23. Espinosa, H.D., Fischer, M., Zhu, Y., and Lee, S. "3-D Computational Modeling of RF MEMS Switches," in Tech. Proc. 4th International Conference on Modeling and Simulation of Microsystems, M. Laudon and B. Romanowicz, eds., 402–405 (2001).

24. Nix, W.D., "Thin Film Reviews – Mechanical Properties of Thin Films," Metall. Trans. A, **20**, *2217–2245 (1989).*

25. Espinosa, H.D., Prorok, B.C., and Fischer, M., "Elasticity, Plasticity and Fracture of Thin Films and MEMS Materials—Part I: A Novel Chip Level Testing Methodology," J. Mech. Phys. Solids, submitted (2001).

26. Chen, S., Baughn, T.V., Yao, Z., and Goldsmith, C., "A New In-situ Residual Stress Measurement Method for MEMS Suspended Membranes," J. Microelectromech. Syst., submitted (2001).

